Structural Analysis of the P10/11-P12 RNA Domain of Yeast RNase P RNA and Its Interaction with Magnesium†

William A. Ziehler,‡ Jonathan Yang,‡ Alexander V. Kurochkin,§ Peter O. Sandusky,‡,|| Erik R. P. Zuiderweg,§ and David R. Engelke*,‡

Department of Biological Chemistry and Biophysics Research Division, The University of Michigan, Ann Arbor, Michigan 48109-0606

Received November 25, 1997; Revised Manuscript Received January 13, 1998

ABSTRACT: The P10/11-P12 RNA domain of yeast RNase P contains several highly conserved nucleotides within a conserved secondary structure. This RNA domain is essential for enzyme function in vivo, where it has a demonstrated role in divalent cation utilization. To better understand the function of this domain, its structure and alterations in response to magnesium have been investigated in vitro. A secondary structure model of the P10/11-P12 RNA domain had been previously developed by phylogenetic analysis. Computer modeling and energy minimization were applied to the *Saccharomyces cerevisiae* P10/11-P12 domain to explore alternatives and additional interactions not predicted by the phylogenetic consensus. The working secondary structure models were challenged with data obtained from ^{1}H NMR and in vitro chemical and enzymatic probing experiments. The solution structure of the isolated domain was found to conform to the phylogenetic prediction within the context of the holoenzyme. Structure probing data also discriminated among additional base contacts predicted by energy minimization. The withdrawal of magnesium does not appear to cause gross refolding or rearrangement of the RNA domain structure. Instead, subtle changes occur in the solution accessibility of specific nucleotide positions. Most of the conserved nucleotides reported to be involved in magnesium utilization in vivo also display magnesium-dependent changes in vitro.

RNase P is a ribonucleoprotein metalloenzyme responsible for processing the 5′ leader of tRNA primary transcripts (*1*−*4*). The bacterial RNase P RNA has been shown to be catalytically competent in vitro, categorizing it as a true ribozyme (*5*). In contrast, eukaryotic nuclear RNase P RNA is not catalytic itself, but is indispensable for functional enzyme in vivo (*6*−*11*). *Saccharomyces cerevisiae* RNase P is composed of a 369 nucleotide transcript in the mature holoenzyme (*11*), and a large but only partially characterized protein contingent (*12*−*15*).

Yeast RNase P RNA has been characterized by comparative phylogenetic sequence analysis. Alignment of yeast covariations and comparison with the bacterial consensus allowed the generation of a secondary structure model (*16*) which was subsequently refined by biochemical structure probing of the RNA within the RNase P holoenzyme (*17*). A key feature of the yeast RNA secondary structure was the P10/11-P12 region which contains several highly conserved nucleotides. Minimization experiments with the yeast RNA have demonstrated that helix P12 is dispensable for in vivo function, but deletion of the loop region containing the CAGAAA sequence is nonviable (*18*). This internal loop structure originally appeared to be unique to yeast (Figure 1) (*16*), although more recent bacterial models now include a similar domain (*19, 20*). The P10/11-P12 domain of the yeast RNA contains the highly conserved internal loop sequence CAGAAA (positions 206−211) at a position comparable to the acAGaRA consensus in the bacterial consensus (*Escherichia coli* positions 130−136; R represents purine, lowercase indicates 80% conserved). Recently, the P10/11-P12 domain and the conserved internal loop structure have been proposed to be the "universal internal loop", comprising part of the conserved core structure of all RNase P RNAs (*21*).

Structural investigation of the *E. coli* RNase P RNA, using distance constraints obtained by photo-cross-linking, has produced a tertiary model of the RNA that positions the P10/11-P12 domain near the tRNA cleavage site (*22*−*24*). These initial models did not predict any interactions between the domain and the tRNA substrate (*25, 26*). However, more recent experiments have identified cross-links between the domain and the tRNA aminoacyl stem (J. Nolan, personal communication). It is therefore quite plausible that this domain has at least a transient interaction with the pre-tRNA substrate.

Several reports have provided evidence that the P10/11-P12 RNA domain is also likely to be involved in magnesium utilization by RNase P. (R_p)-Phosphorothioate interference

† This work was supported by National Institutes of Health Grants NIH GM 34869 and AI 33263. Oligonucleotide synthesis was subsidized by National Institutes of Health Grant P30CA46592 to the University of Michigan Cancer Center. E.R.P.Z. and A.V.K. were partially supported by National Institutes of Health Grant NIH GM 52406. W.A.Z. was supported by the Cellular Biotechnology Training Program, NIH Grant 5T32GM08353.

* Author to whom correspondence should be addressed.

‡ Department of Biological Chemistry.

§ Biophysics Research Division.

|| Present address: Department of Chemistry, Central Michigan University, Mt. Pleasant, MI 48859.

S0006-2960(97)02886-9 CCC: $15.00
Published on Web 02/20/1998

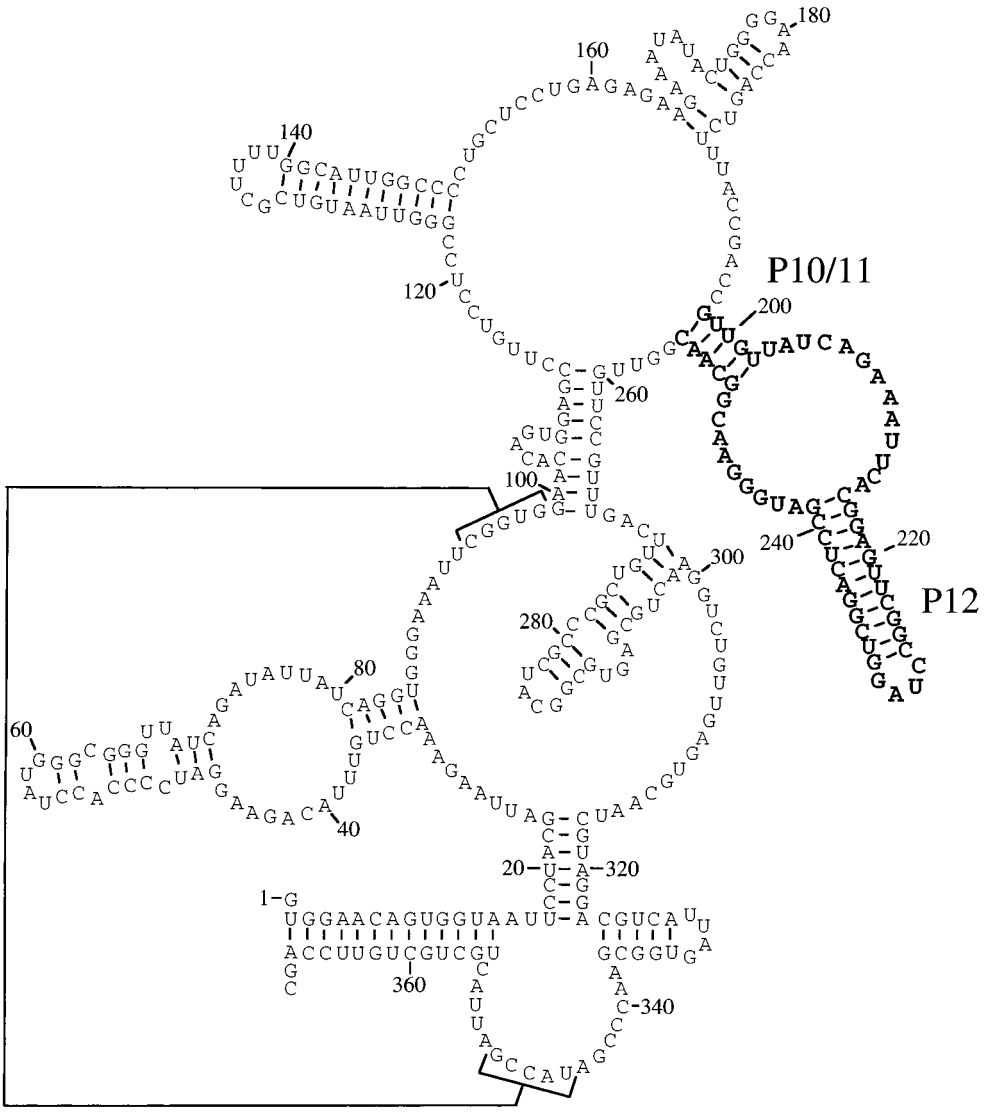

FIGURE 1: Secondary structure of yeast nuclear RNase P RNA. The P10/11-P12 domain, shown relative to the proposed secondary-structure (*17*), is in bold.

and manganese rescue studies showed that binding of substrate to *E. coli* RNase P RNA requires divalent cation-mediated interactions with the conserved loop (*27*). In addition, magnesium at alkaline pH (*28*) and lead-induced hydrolysis (*29*) both cleave the bacterial RNA at several positions in the domain. Characterization of viable mutations in the CAGAAA sequence of this domain in yeast also suggested a function in magnesium utilization (*20*). Kinetic analysis of the mildly defective holoenzymes showed that mutations affected primarily catalytic rate (k_{cat}), with little change in apparent substrate binding (K_m). It was also observed that several holoenzymes with variant, but viable, CAGAAA sequences had 2- to 6-fold increases in the magnesium concentration required for half-maximal activity.

These observations implicate the P10/11-P12 domain in an interaction with one or more magnesium ions and suggest that the domain may be part of the active site. The present study is intended to probe the structure of the domain and the response of that structure to magnesium.

EXPERIMENTAL PROCEDURES

Computer Prediction of P10/11-P12 RNA Domain Secondary Structure. Alternate structures to the P10/11-P12 RNA domain phylogenetic consensus were generated using Mfold (M. Zuker, http://www.ibc.wustl.edu/~zuker/rna/form1.cgi). The user defined parameter "percent suboptimality" was set from 5% to 50% (http://www.ibc.wustl.edu:8000/~zuker/rna/form1-doc.html#PERCENT), and the "window" was set from 1 to 5 (http://www.ibc.wustl.edu:8000/~zuker/rna/form1-doc.html#WINDOW) (*50*, *51*).

Eight unique structures were obtained; however, only two (Figure 3) were in approximate agreement with the phylogenetic data.

RNA Synthesis. The P10/11-P12 domain RNA and a P10/11-P12−tRNA fusion transcript were generated as previously described (*30*). Briefly, DNA encoding the P10/11-P12 domain was inserted between the T7 RNA polymerase promoter and a tRNA gene ($tRNA^{Asp}$, provided by C. Reich and N. Pace, Indiana University). Template for in vitro transcription was amplified by PCR. Transcription with T7 RNA polymerase results in a fusion transcript that can be processed by *E. coli* RNase P RNA (M1 RNA) to produce a discrete P10/11-P12 domain RNA with a 3′-OH and a mature tRNA. The two products are purified by denaturing acrylamide gel electrophoresis. The P10/11-P12 domain was treated with bacterial alkaline phosphatase (Gibco BRL),

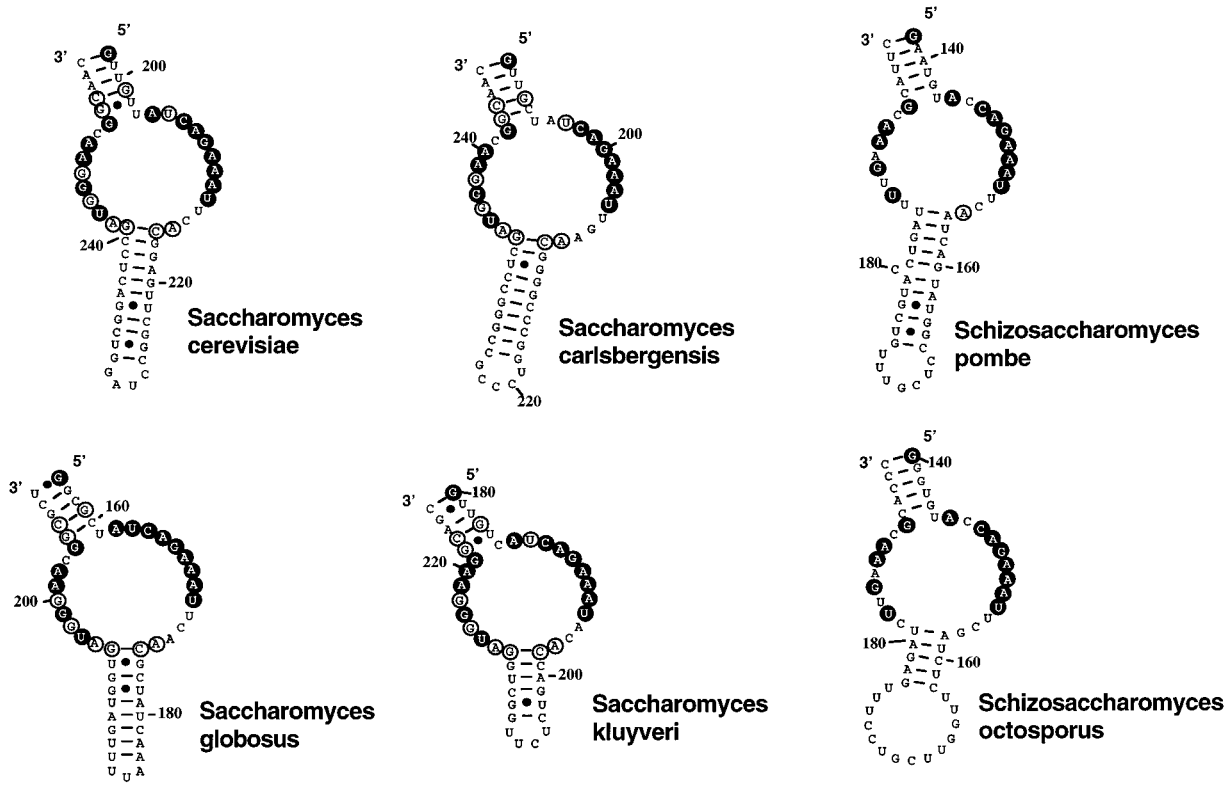

FIGURE 2: P10/11-P12 domain nuclear RNAs from six yeast species. Absolutely conserved nucleotides (*16*) are indicated by filled circles, and nucleotides with ≥80% conservation are indicated by open circles.

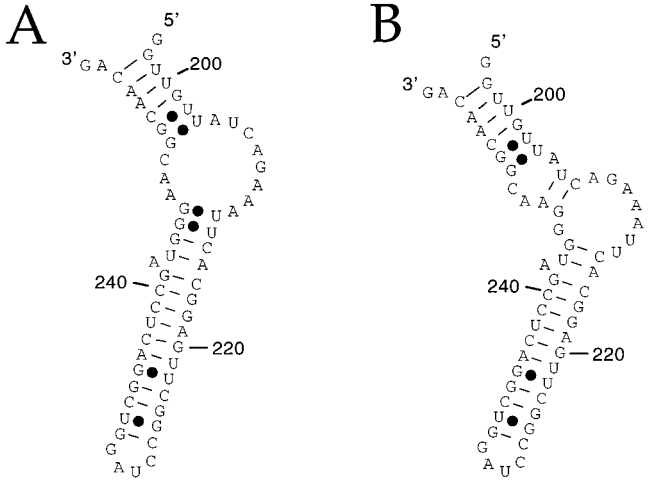

FIGURE 3: Computer-derived secondary structures of the P10/11-P12 domain nuclear RNA from *S. cerevisiae*. The structures depicted are selected from eight candidates predicted by Mfold (M. Zuker, http://www.ibc.wustl.edu/~zuker/rna/form1.cgi) to contain the phylogenetically conserved P10/11 and P12 helices in Figure 2. Variation in nucleotide base-pairing is constrained to be within the internal loop region.

isolated, and labeled using T4 polynucleotide kinase (Boehringer Mannheim) and [γ-^{32}P]ATP (NEN).

All RNA species were refolded after purification in glass-distilled water with 10 mM Tris pH 7.5, except that the DMS and KE reactions contained 50 mM HEPES pH 7.9. The sample was heated to >90 °C for 2 min and rapidly cooled in an ice bath. Potassium chloride and magnesium chloride were then added. Native polyacrylamide gel electrophoresis of intact and M1-processed fusion transcripts demonstrated that each RNA migrated as a single band. Slow cooling and/or the presence of mono- and/or divalent cations allowed for dimerization of the RNAs due to extensive self-complementarity of the P10/11-P12 domain.

^{1}H NMR. Spectra were taken on a Bruker AMX 500 MHz spectrometer. A Jump-Return followed by a Watergate sequence was used for superior H_2O suppression which keeps the H_2O resonance in $+z$. The samples used in these experiments consisted of 200 μM RNA in 50 mM deuterated Tris buffer pH 7.0 with 8 mM $MgCl_2$ and 100 mM KCl. During the temperature study of this spectrum, an initial spectrum of the sample equilibrated at 25 °C was taken, and the temperature was then raised in 5 °C increments for each subsequent spectrum. The sample was equilibrated for 30 min at each temperature.

Assignment spectra for this fragment were obtained at 20 °C on a Bruker AMX600 spectrometer equipped with an 8 mm Nalorac gradient probe. Assignments were obtained from a combined analysis of NOESY spectra in H_2O with 75, 200, and 400 ms NOE mixing times, a NOESY spectrum in ^2H_2O with 100 ms mixing time, a TOCSY spectrum in ^2H_2O with 40 ms mixing time, and 1D spin−echo spectra in ^2H_2O (*31*). Excellent and very stabile solvent suppression was obtained by a Jump-Return Watergate sequence as NOE-mixing time readout. NOESY and TOCSY spectra were collected for 36 h each.

Chemical and Enzymatic Structure Probing. Structure probing of the P10/11-P12 domain RNA and fusion RNA was performed in final $MgCl_2$ concentrations of 0, 20, 100, and 500 μM, and 1, 3, 6, 10, and 50 mM. An additional reaction in 1 mM EDTA was used to probe structure in the absence of contaminating divalent cations. The chemical and enzyme reactions are based in part on methods described elsewhere (*32, 33*).

Structure probing of the 5′ end-labeled P10/11-P12 domain RNA was accomplished with the following reagents, with cleavage or modification preferences indicated in parentheses: RNase V1 [double-stranded (ds) RNA], RNase T1 [single-stranded (ss) G], RNase A (ss C and U), RNase Phy M (A and U), RNase CL3 (C predominantly), RNase I (ss), $PbCl_2$ (preferentially ss RNA phosphates, Otzen et al., ref *49*), dimethyl sulfate (N-7-G), and diethyl pyrocarbonate (N-7-A). RNase V1 was used only with 10 mM Mg^{2+}, as its activity is divalent cation-dependent. DMS and DEPC modifications were reduced with $NaBH_4$ and treated with aniline as described (*33*). The reaction mixture for each reagent contained 10 mM Tris pH 7.5, 100 mM KCl, and 10 μM unlabeled RNA + 5′-^{32}P-labeled RNA. Samples were incubated at room temperature for 30 min. Chemical or nuclease dilution was added and allowed to react for 10 min. Reactions were precipitated with ethanol and resuspended in formamide, and the products were resolved on denaturing polyacrylamide gel electrophoresis. Reagents were individually titrated to cleave or modify approximately 10% of the total P10/11-P12 domain RNA substrate. Alkaline hydrolysis and denaturing RNase T1 digests of ^{32}P-labeled P10/11-P12 domain RNA provided size markers (*32*), and RNA samples minus reagent were used as cleavage/modification controls.

A P10/11-P12 domain RNA-tRNA fusion transcript was probed with dimethyl sulfate (DMS, N-1 of adenosine and N-3 of cytosine) and kethoxal (KE, N-1 and NH_2-2 of guanosine) to determine Watson−Crick position accessibilities. Reactions contained 50 mM HEPES pH 7.9, 100 mM KCl, variable $MgCl_2$, and 10 μM fusion RNA. After 30 min at room temperature with $MgCl_2$, DMS or KE was added and allowed to incubate for 30 min. Reactions were stopped by ethanol precipitation on dry ice. Primer extension reactions were performed using the oligo 5′ CCC GCG ACC TCC TGC GTG ACA GGC AGG CAT TCT AAC CAA C 3′, labeled with ^{32}P by T4 polynucleotide kinase (Boehringer Mannheim), and Superscript II (Gibco BRL) reverse transcriptase. Products were resolved on denaturing polyacrylamide sequencing gels alongside dideoxynucleotide sequencing reactions as markers. Primer extension on unmodified RNA identified reagent-independent terminations.

Phosphorimager Analysis. Reaction products were visualized using a phosphorimager (model 445 SI, Molecular Dynamics) and quantitated using ImageQuant software (Molecular Dynamics). Location of modifications and cleavages was determined by comparison with the standard reactions (i.e., base hydrolysis and denaturing RNase T1 for 5′ labeled RNA, dideoxynucleotide sequencing for primer extension). Line scan profiles were examined to locate magnesium-dependent intensity changes. Only changes greater than 50% were considered magnesium-sensitive. Changes from 50% to greater than 300% were observed across the magnesium titrations for the reagents shown in Figure 7.

RESULTS

Secondary Structure Modeling. Phylogenetic analysis of the P10/11-P12 domain predicted a largely unpaired internal loop in the functional form of the enzyme (Figure 2). To help evaluate the folding of the isolated domain and the degree to which divalent cations affect that structure, multiple

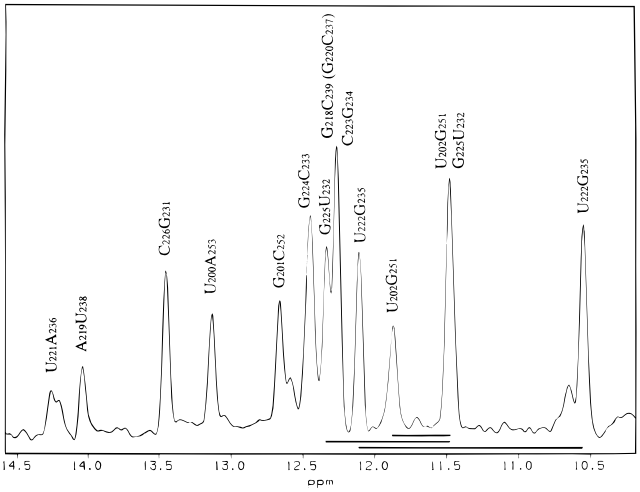

FIGURE 4: 600 MHz Imino proton NMR spectrum for the P10/11-P12 RNA domain (20 °C, pH 7.5) Assignments indicated were obtained from NOESY, TOCSY, and spin echo data sets. The horizontal lines identify the two imino protons belonging to the UG wobble pairs.

predicted structures were obtained from the Mfold energy minimization folding algorithm (M. Zuker, http://www.ibc.wustl.edu/~zuker/rna/form1.cgi). Two structures, of a total eight predictions, in agreement with the yeast consensus prediction are shown in Figure 3. These models were intended to predict alternative, less stable interactions that might identify a unique secondary structure not suggested by the genetic data. The Mfold structures also provide clues for alternates to be evaluated by the biochemical data. The internal loop in Figure 2 contains several highly conserved nucleotides, and it is this portion of the domain that was examined for potential structure using computer predictions based on energy minimization. Several nucleotides within the loop region have pairing potential, and such interactions might exist in solution despite a lack of phylogenetic support.

Computer predictions provided two alternatives that are consistent with phylogenetic predictions and near subsequent experimental determination (Figure 3). The P10/11 and P12 helices are preserved, with differences occurring in the internal loop. These structures provided hypotheses for alternate interactions to be examined using NMR and biochemical techniques.

^{1}H NMR. The ^{1}H NMR spectrum of the 60 base (G197 to G257) P10/11-P12 domain shows 15 resolved hydrogen-bonded imino peaks in the spectral region between 9.5 and 15 ppm (Figure 4).

Assignments of imino protons from stable base-pairs at 20 °C are indicated in Figure 4. Very strong NOE cross-peaks between imino protons in the spectral range 9.5−12.5 ppm identified U−G base-pair imino protons (*31*). One-dimensional spin−echo spectra revealed the frequencies of the adenosine H2 resonances, which then by very strong NOEs to the uridine imino protons identified the latter. AU base-pairs were further identified by considering the characteristic relative paucity of imino-to-amino cross-peaks. The remaining imino protons were assigned to GC base-pairs, which were further characterized by identification of guanine imino-cytosine H6/H5 spin diffusion cross-peaks. The latter resonances were identified from the TOCSY data set. The sequence-specific assignments were subsequently obtained

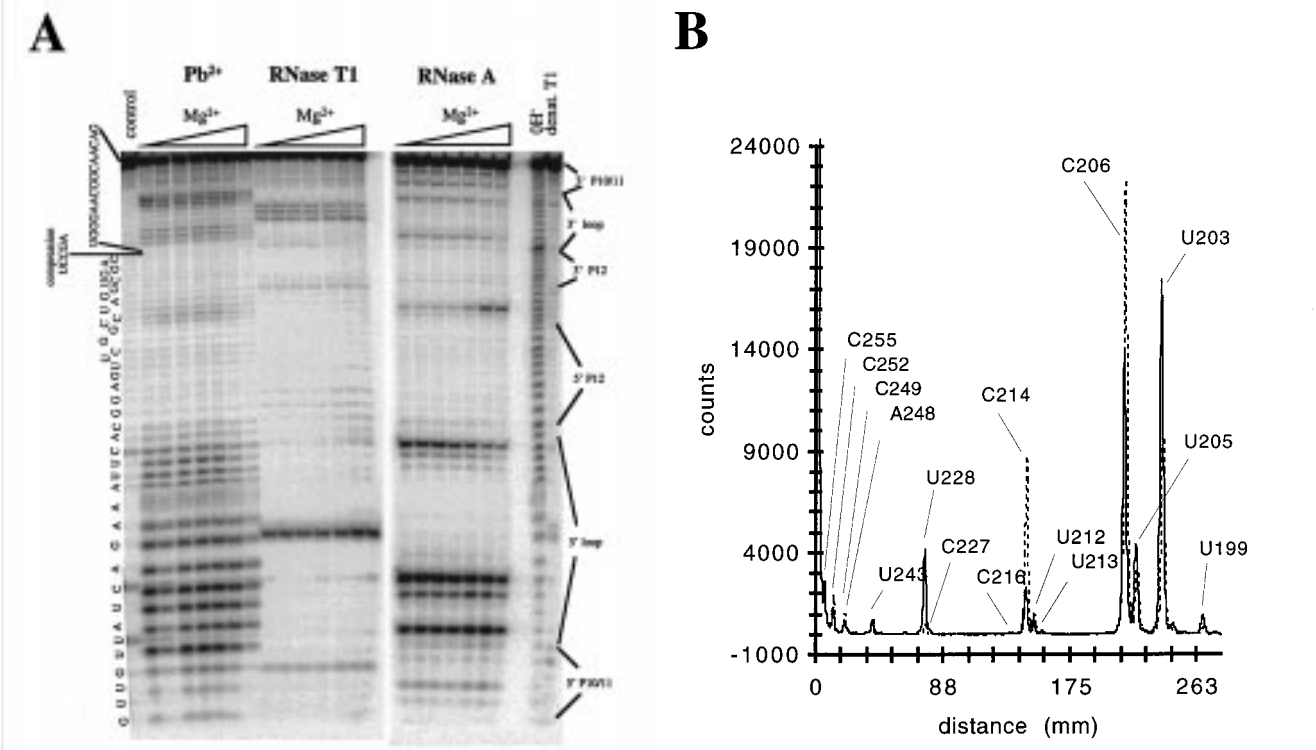

FIGURE 5: Examples of structure-probing experiments incorporating variable magnesium concentrations. (A) Phosphorimager scans of denaturing polyacrylamide gels are shown. Pb^{2+}, RNase T1, and RNase A are shown with 1 mM EDTA, and 0, 20, 100, and 1, 10, 50 mM $MgCl_2$. (B) Line scan from phosphorimager analysis of RNase A, the two traces compare the digestion profiles for 20 μM (dashed line) and 10 mM (solid line) $MgCl_2$.

from tracing the (very) weak imino-imino proton NOEs. Unambiguous and contiguously linked assignments were obtained for the stem region U221/A236 to C226/G231. The other indicated assignments were obtained as blocks of two or three sequentially linked imino proton signals. The placement in the sequence for these resonances is compatible with the base-pairing schemes as drawn in Figures 3B and 7A−E. The assignment of these resonances would have been ambiguous if not for later chemical and enzyme probing data: the three base-pair stem U200/A253-G201/C252-U202/G249 could also be placed at the location A215/U243-C214/G244-U213/G245 (see Figures 2 and 3A). However, when the data from Figure 6 is considered, it rules out the base-pairing scheme of Figure 3a. The assignments in Figure 4 are therefore the most probable. It is also likely that this helix is unstable, since between 35 and 45 °C two peaks corresponding to the hydrogen-bonded imino protons of U200/A253 and G201/C252 in the short P10/11 helix disappear from the spectrum. Resonances corresponding to the P12 hairpin helix broaden and disappear at significantly higher temperatures, between 55 and 70 °C.

Biochemical Structural Analysis. Determination of accessibility to chemical and enzymatic reagents was used to challenge working secondary structure models of the P10/11-P12 domain RNA. Two P10/11-P12 domain RNA species were used, a 5′ ^{32}P-labeled domain RNA to detect cleavage events, and a P10/11-P12 domain−tRNA fusion that could be used to detect Watson−Crick position modifications by primer extension. The results of probing experiments will initially be described for RNA in the presence of 100 mM KCl and 4 mM $MgCl_2$. The next section will discuss differences detected in the structure as the concentration of Mg^{2+} is varied from 0 to 50 mM.

The 5′ ^{32}P-labeled P10/11-P12 domain RNA was probed with DMS, DEPC, Pb^{2+}, RNases A, T1, I, Phy M, and CL3 for single-stranded nucleotides, and RNase V1 for double-stranded regions. Each reagent was used in conjunction with a titration of Mg^{2+} to identify modification/cleavage sites sensitive to the concentration of the metal. Nucleic acid structure is stabilized in many instances in the presence of divalents (*34*). The exception was RNase V1, which was used only in 10 mM Mg^{2+} because its activity is strongly dependent on divalent cations.

Accessible Watson−Crick positions were probed using a P10/11-P12−tRNA fusion RNA (Figure 6F), (*30*) with dimethyl sulfate (DMS) and kethoxal (KE). Access to both reagents was examined throughout a Mg^{2+} titration to locate positions sensitive to divalent concentrations. The independently folding tRNA provides a DNA oligomer binding site, but does not significantly interfere with folding of the P10/11-P12 domain. This is evidenced by the fact that DMS and KE modifications, with two exceptions, match those in the context of the holoenzyme (*17*). One of these exceptions is A_{242}, which is lightly modified in the holoenzyme, but not modified in the P10/11-P12−tRNA fusion. Also, the P10/11 helix can be penetrated by the modifying agents in the fusion RNA, whereas this region is inaccessible in the holoenzyme. It is possible that the unnatural 5′ end of the P10/11 helix in the fusion RNA reduces structural constraints present in the holoenzyme, thereby allowing the observed modifications. Similarly, A_{242} might have an altered environment in the fusion RNA.

Examples of cleavage products are shown in Figure 5A for Pb^{2+}, RNase T1, and RNase A. An example of comparative phosphorimager quantitation of reaction products is shown in Figure 5B. Location and approximate

intensities of modification/cleavage sites for the 5′ ^{32}P-labeled P10/11-P12 domain RNA and the P10/11-P12−tRNA fusion RNA (in the presence of >1 mM Mg^{2+}) are shown in Figure 6. Most reagents hit within the internal loop region defined by the phylogenetic structure. This portion of the RNA is consistently more accessible and is likely to lack stable Watson−Crick pairing. This does not discount the possibility of unconventional base-pairing interactions within the loop, but any such pairings are unable to prevent nucleotide-specific RNase recognition as well as modification of Watson−Crick positions by DMS and KE. There are two exceptions, A_{215} and A_{242}, which are at the base of the P12 helix. Neither adenosine was cleaved by RNase Phy M or modified by DMS, whereas all other nucleotides in the loop were accessible to one or more of the nucleotide-specific reagents. None of the base-specific nucleases was able to hit all of its potential targets within the loop, possibly due to steric constraints produced by portions of the P10/11-P12 domain's structure. Conversely, the small molecules, DMS and KE, hit all of their potential nucleotide targets within the loop region, except A_{215} and A_{242}. Thus, these bases might be involved in hydrogen bonding in the loop structure.

RNase V1 cleaves at U_{221}, U_{222}, and G_{241}, supporting the existence of the P12 helix. The lack of cleavages in the proposed P10/11 helix suggests that this structure might be too short or unstable to be recognized by V1.

Reagents that are not nucleotide-specific, RNase I and Pb^{2+}, were used to probe for general secondary structure characteristics. RNase I cleaves 3′ to single-stranded nucleotides, and its cleavage pattern in the internal loop and terminal hairpin loop is consistent with the phylogenetic model. It also cleaves after U_{200}-U_{202}, consistent with instability of the P10/11 helix. It is curious that their proposed base-pairing partners, G_{251}-A_{253}, are not cleaved and that C_{249} and G_{250} are also not cleaved. Upon comparison with other reagents, the inaccessibility of C_{249}-A_{253} is likely due to a specific blockage of RNase I to these nucleotides, since RNase A and RNase T1 are able to access C_{249}-A_{253}. Therefore, it is more likely that the short P10/11 helix has at least transient single-strand character under the conditions assayed, permitting penetration by some reagents. This would be consistent with the observed thermal instability of the short helix in the NMR.

Hydrolysis by Pb^{2+} occurs preferentially in single-stranded regions (*35*) and should not have the same steric constraints as RNase I, yet Pb^{2+} does not cleave after the loop nucleotides C_{249}-G_{251}, or within the potentially weak P10/11 helix. Phosphates within the P10/11 helix and following C_{249}-G_{251} appear to be inaccessible to cleavage by Pb^{2+}, suggesting that they are double-stranded or in a tertiary structure that inhibits cleavage.

Strong cleavages by Pb^{2+} (filled circles, Figure 6E) are compatible with the prediction in Figure 3A, providing the only support for the alternate structure. It is possible that Pb^{2+} might be inducing and/or stabilizing this alternate RNA structure. However, the proposed pairing partners of nucleotides U_{203}-U_{205} and the majority of the loop phosphates are accessible to Pb^{2+}. Thus, only a small population of alternate structure RNAs exist, if at all. The Pb^{2+} cleavage pattern is generally more indicative of the phylogenetic model than the Figure 3A alternate.

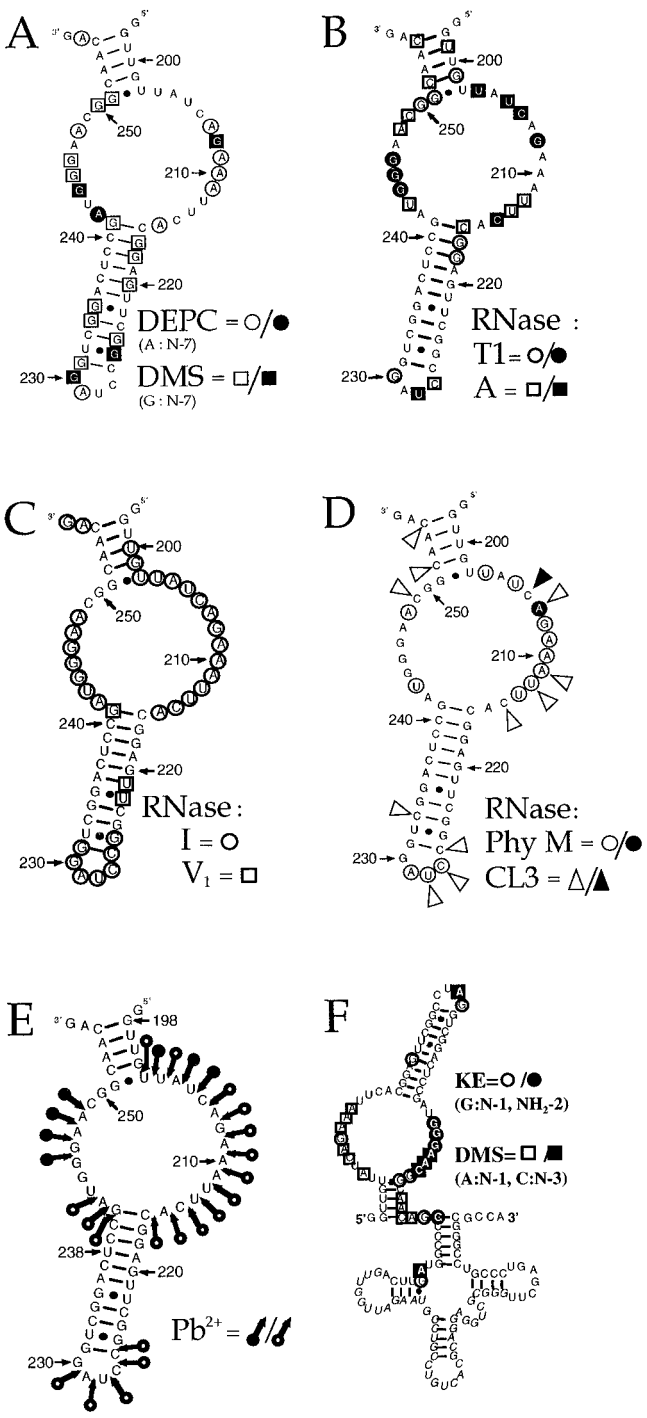

FIGURE 6: Summary of chemical and enzyme accessibilities in the presence of 1 mM $MgCl_2$. (A) DMS and DEPC N-7 modifications, (B) RNases A and T1, (C) RNases V1 and ONE, (D) RNases Phy M and CL3, (E) Pb^{2+}, (F) DMS and KE Watson−Crick modifications detected by primer extension using the P10/11-P12 domain RNA fused to a tRNA; the DNA oligo primer is complementary to the italicized nucleotides contained in the tRNA. Strong modifications or cleavages are indicated by filled symbols and weak ones are indicated by open symbols.

The small organics, DMS and DEPC, were used to probe the N-7 of guanosines and adenosines, respectively. There is evidence of metal ion interactions with the N-7 of purines in the hammerhead ribozyme crystal structure (*36*) and nucleotide crystals (*37*). Several noncanonical base-pairing interactions are also possible that involve the N-7 position (*38*). However, Figure 6A shows that most purine N-7s in

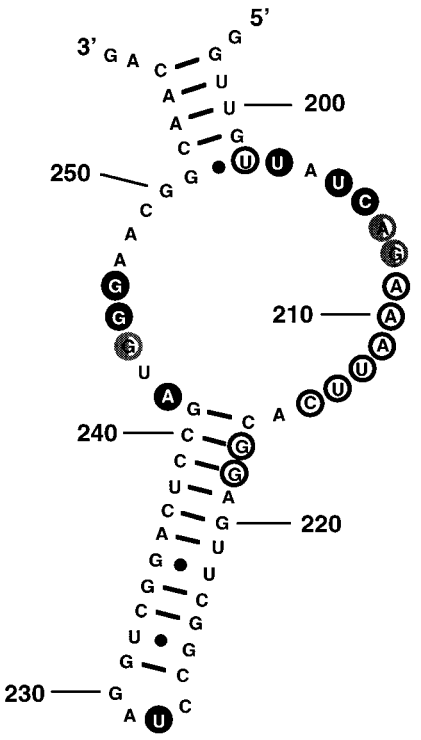

Reagent	Nucleotide	Accessibility change with added Mg^{2+}
RNase I	U_{203}	+
	G_{208}	-
	$A_{209 - 211}$	- -
	$U_{212 - 213}$	- -
RNase CL3	U_{203}	+ +
	C_{206}	+
	A_{207}	+
	A_{211}	- - -
	U_{212}	- -
	C_{214}	- -
RNase PhyM	U_{205}	+ +
	A_{207}	-
RNase A	C_{214}	- - -
	U_{228}	+ + +
RNase T_1	G_{208}	+
	G_{244}	+
DMS(G:N-7)	$G_{217 - 218}$	-
	G_{244}	-
DEPC	A_{242}	+ +
Pb^{2+}	U_{202}	- -
	A_{211}	-
	$U_{212 - 213}$	- -
	C_{214}	-
KE	G_{208}	+
	$G_{244 - 246}$	+ +

FIGURE 7: Nucleotides with magnesium-sensitive modifications or cleavages. Relative accessibilities are listed by reagent. Accessibility changes were observed from 50 to 300%, and the relative extent of the change is indicated by (+) or (−) = 50−100%, (++) or (--) = 100−200%, and (+++) or (---) = 200−300% changes. Filled circles indicate nucleotides which are more accessible with increasing magnesium, open circles indicate nucleotides that are less accessible with increasing magnesium. Half-filled circles are nucleotides which displayed both effects, depending on the reagent employed.

the internal loop and P12 regions of the RNA are accessible to these reagents. Two interesting exceptions are A_{204} and A_{247}. These two adenosines are candidates for hydrogen-bonded interactions. Also, neither position is reactive toward RNase A or RNase Phy M, which require nucleotide recognition. There are several potential noncanonical pairing partners in the loop for each adenosine, including the possibility that they interact with each other. A second option, that one or both of these adenosines is directly or indirectly involved in Mg^{2+} coordination, is an intriguing possibility.

There are a few instances of enzymes cleaving at uncharacteristic nucleotides. RNase A weakly cleaves at A_{248}, and RNase Phy M cleaves at G_{208} and C_{227}. They do not appear to be breakdown products in the control RNA; but their interpretation in the structure analysis is not clear. It is possible that these uncharacteristic hits are a result of increased accessibility and/or specific structure that makes these nucleotides especially labile.

The P10/11-P12 domain RNA was also probed with hydroxyl radicals using both hydrogen peroxide (*39*) and molecular oxygen (*40*) protocols (data not shown). The reactions contained the same magnesium titration used with the chemical and enzyme reagents. Each method resulted in a uniform cleavage pattern similar to that produced by base hydrolysis. Line scan quantitation by phosphorimager analysis confirmed there were no clearly favored or protected regions of the RNA. It was concluded that the P10/11-P12 domain lacks strong tertiary structure that buries part of the molecule in solution-inaccessible pockets.

Magnesium-Dependent Changes in Reagent Accessibility. The experiments reported above for accessibility to cleavage or modification were carried out at magnesium concentrations appropriate for maximal activity of the RNase P holoenzyme. To probe sensitivity of the domain structure to magnesium, changes in accessibility were mapped while increasing magnesium from 0 μM (1 mM EDTA) to 50 mM (Figure 7). Only reproducible changes equal to or greater than 50% are reported; the relative magnitude of each magnesium-sensitive cleavage or modification is indicated in Figure 7. Most of the conserved CAGAAA sequence, including a few adjacent nucleotides, is relatively protected as the concentration of magnesium increases. This region displays the strongest reductions, with hits between A_{209} and C_{214} decreased by 100−300%. The conserved CAGAAA sequence and neighboring nucleotides are, therefore, likely to adopt an inaccessible structure induced by magnesium. The N-7 positions of P12 helix guanosines in the 5′ side of the helix also experience a reduction in accessibility. Again, this reduction could be due to tighter structure forming in the loop region stabilizing the beginning of the P12 helix or altering the helical parameters such that the major groove affords less access to DMS. In contrast, positions U_{203}, U_{205}, C_{206}, U_{228}, A_{242}, G_{245}, and G_{246} become hypersensitive to nucleases and modification at Watson−Crick positions as the magnesium concentration increases, consistent with increased accessibility to the solution.

Some nucleotides showed opposite changes in sensitivity depending on the reagent employed. These are indicated by half-filled circles in Figure 7. A_{207} is more accessible to

RNase CL3, though CL3 is reported to be specific for cytosine. Aside from the CL3 cleavage, A_{207} decreases in accessibility overall, and could be indicated by an open circle in Figure 7. G_{208} also has an atypical cleavage by RNase Phy M, and this sensitivity decreases in the presence of Mg^{2+}. RNase I cleavage of G_{208} also decreases, but RNase T1 cleavage and KE modification increase, which suggest the Watson−Crick determinants are more available. Last, G_{244} is more accessible to RNase T1 and KE as the [Mg^{2+}] is increased, but its N-7 becomes less accessible to DMS, indicating that the G_{208} Watson−Crick determinants are more available in the presence of magnesium but the major groove is not.

DISCUSSION

The present analysis allowed confirmation of the phylogenetic structure of the yeast P10/11-P12 domain RNA. Least energy predictions suggest the possibility of extended base-pairing across the loop region of the RNA. Secondary structure models were evaluated with data obtained from ^{1}H NMR and biochemical structure probing. The NMR and biochemical data revealed that the domain structure is generally limited to the phylogenetic prediction. Last, the RNA cleavage and modification reagents show significant changes in response to increased Mg^{2+}, especially in the loop region. These include many of the conserved nucleotides found to affect Mg^{2+} utilization by yeast RNase P in vivo (i.e., C_{206}−A_{211}). The same nucleotides also demonstrate reduced accessibility to the structure probing reagents in the presence of Mg^{2+}, while ones adjacent and across the loop become more accessible.

The NMR data also show that the large P12 helix is formed in solution. No evidence is found for extensive secondary structure involving bases of the loop area. Indeed, the observation of only 15 strong imino proton resonances for a 61 base-RNA fragment indicates a lack of stable secondary structure for a very large part of the molecule. The NMR temperature data indicate that the P12 helix is more stable than the short P10/11 helix.

There are several potential roles for the P10/11-P12 RNA domain. Previous data suggest that the domain is responsible for interacting with one or more Mg^{2+} ions and directly or indirectly affects the catalytic rate. The present study shows that many of the conserved nucleotides become less accessible with increasing Mg^{2+} concentration over the range required for optimal RNase P activity. This might be an indication of a metal "footprint". For example, direct interaction of the CAGAAA sequence with Mg^{2+} might result in relative protection from the probing reagents. The Pb^{2+} cleavage data also suggest that divalent metal binding is localized in the loop region of the RNA, and, as the amount of Mg^{2+} is reduced, Pb^{2+} gains more access to A_{211} and several bases adjacent to the conserved CAGAAA sequence. Alternatively, interaction of the divalent metal with the RNA could cause structural changes that indirectly result in the sensitivity changes. There does not appear to be direct base-pairing across the loop region with the addition of Mg^{2+}, as suggested by the thermodynamically derived structures in Figure 3, but it is clear that portions of the internal loop change their accessibility to reagents.

The accessibility of all positions in the CAGAAA sequence is influenced by the amount of Mg^{2+} present, suggesting a role in establishing a structure that interacts with Mg^{2+}. We have previously shown that mutations in this sequence increase the magnesium requirement of the RNase P holoenzyme, and that this effect is primarily on k_{cat}. The experiments in the present study show the domain structure is sensitive to $MgCl_2$ concentration within the same range (1−10 mM).

Comparison of this domain in yeast and bacteria shows that the P10/11 helices in both cases are relatively unstable. The P10 and P11 helices of the bacterial RNA are very short (2 nucleotides) and are separated by an asymmetric bulge. This is consistent with the apparent instability of the yeast P10/11 helix and suggests that the instability might serve a purpose in the enzyme. Resulting flexibility might allow the entire domain to move in relation to the rest of the RNase P RNA and bound tRNA substrate. The P10/11-P12 domain could thus make structural transitions with the substrate and/or the RNase P active site architecture. It has been reported that the bacterial RNA retains a very low remnant of catalytic activity in vitro upon deletion of the highly conserved P10/11-P12 domain (*41*), although this is true only in extreme monovalent and divalent concentrations (2 M NH_4OAc, 400 mM $MgCl_2$, Y. Lee, personal communication). One possible function for this domain might be to efficiently present metal ion(s) to the active site at physiological concentrations of magnesium. To carry out such a function, considerable movement of the domain might be required relative to the immobilized substrate.

It is worth noting that a sequence similar to the RNase P acAGaRA consensus also exists in the central domain of U6 small nuclear RNA in eukaryotes (*42*−*45*). The invariant U6 ACAGAGA sequence is located in the catalytic heart of the spliceosome and cross-links to the 5′ splice junction in pre-mRNA (*45*). The mechanisms of RNase P cleavage and pre-mRNA splicing use different nucleophiles; however, both are proposed to involve S_N2 attack by a hydroxyl group on the scissile phosphodiester bond to generate 3′-hydroxyl termini (*5*, *43*, *46*−*48*). In addition, both would be compatible with a proposed two metal ion mechanism (*48*). The structure of this isolated RNase P domain might therefore provide insights into a motif that is used more broadly in biological processes.

ACKNOWLEDGMENT

We thank Dr. James Nolan for communicating results prior to publication.

REFERENCES

1. Altman, S. (1989) *Adv. Enzymol. 62*, 1−36.
2. Pace, N. R., and Smith, D. (1990) *J. Biol. Chem. 265*, 3587−3590.
3. Darr, S. C., Brown, J. W., and Pace, N. R. (1992) *Trends Biochem. Sci. 17*, 178−182.
4. Chamberlain, J. R., Tranguch, A. J., Pagán-Ramos, E., and Engelke, D. R. (1996) in *Progress in Nucleic Acids Research and Molecular Biology* (Moldave, K., and Cohn, W., Eds.) pp 87−119, Academic Press, New York.
5. Guerrier-Takada, C., Gardiner, K., Marsh, T., Pace, N., and Altman, S. (1983) *Cell 35*, 849−857.
6. Miller, D. L., and Martin, N. C. (1983) *Cell 34*, 911−917.
7. Doersen, C. J., Guerrier Takada, C., Altman, S., and Attardi, G. (1985) *J. Biol. Chem. 260*, 5942−5949.
8. Krupp, G., Cherayil, B., Frendewey, D., Nishikawa, S., and Soll, D. (1986) *EMBO J. 5*, 1697−1703.

9. Cherayil, B., Krupp, G., Schuchert, P., Char, S., and Soll, D. (1987) *Gene 60*, 157−161.
10. Lee, J. Y., and Engelke, D. R. (1989) *Mol. Cell. Biol. 9*, 2536−2543.
11. Lee, J. Y., Rohlman, C. E., Molony, L. A., and Engelke, D. R. (1991) *Mol. Cell. Biol. 11*, 721−730.
12. Lygerou, Z., Mitchell, P., Petfalski, E., Seraphin, B., and Tollervey, D. (1994) *Genes Dev. 8*, 1423−1433.
13. Chu, S., Zengel, J. M., and Lindahl, L. (1997) *RNA 3*, 382−391.
14. Dichtl, B., and Tollervey, D. (1997) *EMBO J. 16*, 417−429.
15. Stolc, V., and Altman, S. (1997) *Genes Dev. 11*, 2414−2425.
16. Tranguch, A. J., and Engelke, D. R. (1993) *J. Biol. Chem. 268*, 14045−14055.
17. Tranguch, A. J., Kindelberger, D. W., Rohlman, C. E., Lee, J. Y., and Engelke, D. R. (1994) *Biochemistry 33*, 1778−1787.
18. Pagán-Ramos, E., Tranguch, A. J., Kindelberger, D. W., and Engelke, D. R. (1994) *Nucleic Acids Res. 22*, 200−207.
19. Haas, E. S., Brown, J. W., Pitulle, C., and Pace, N. R. (1994) *Proc. Natl. Acad. Sci. U.S.A. 91*, 2527−2531.
20. Pagán-Ramos, E., Lee, Y., and Engelke, D. R. (1996) *RNA 2*, 1100−1109.
21. Chen, J. L., and Pace, N. R. (1997) *RNA 3*, 557−560.
22. Harris, M. E., Nolan, J. M., Malhotra, A., Brown, J. W., Harvey, S. C., and Pace, N. R. (1994) *EMBO J. 13*, 3953−3963.
23. Westhof, E., and Altman, S. (1994) *Proc. Natl. Acad. Sci. U.S.A. 91*, 5133−5137.
24. Pagán-Ramos, E., Tranguch, A. J., Nolan, J. M., Pace, N. R., and Engelke, D. R. (1995) *Nucleic Acids Symp. Ser. 33*, 89−91.
25. Burgin, A. B., and Pace, N. R. (1990) *EMBO J. 9*, 4111−4118.
26. Nolan, J. M., Burke, D. H., and Pace, N. R. (1993) *Science 261*, 762−765.
27. Hardt, W. D., Warnecke, J. M., Erdmann, V. A., and Hartmann, R. K. (1995) *EMBO J. 14*, 2935−2944.
28. Kazakov, S., and Altman, S. (1991) *Proc. Natl. Acad. Sci. U.S.A. 88*, 9193−9197.
29. Ciesiolka, J., Hardt, W. D., Schlegl, J., Erdmann, V. A., and Hartmann, R. K. (1994) *Eur. J. Biochem. 219*, 49−56.
30. Ziehler, W. A., and Engelke, D. R. (1996) *BioTechniques 20*, 622−624.
31. Wemmer, D. E. (1992) in *Biological Magnetic Resonance* (Berliner, L. J., and Reuben, J., Eds.) Vol. 10, pp 195−290, Plenum Press, New York.
32. Knapp, G. (1989) *Methods Enzymol. 180*, 192−212.
33. Krol, A., and Carbon, P. (1989) *Methods Enzymol. 180*, 212−227.
34. Jaeger, J. A., SantaLucia, J., Jr., and Tinoco, I., Jr. (1993) *Annu. Rev. Biochem. 62*, 255−287.
35. Zito, K., Huttenhofer, A., and Pace, N. R. (1993) *Nucleic Acids Res. 21*, 5916−5920.
36. Scott, W. G., Murray, J. B., Arnold, J. R. P., Stoddard, B. L., and Klug, A. (1996) *Science 274*, 2065−2069.
37. Barton, J. K., and Lippard, S. J. (1980) in *Nucleic Acid-Metal Ion Interactions* (Spiro, T. G., Ed.) pp 34−113, John Wiley & Sons, New York.
38. Tinoco, I. (1993) in *The RNA World* (Gesteland, R. F., and Atkins, J. F., Eds.) pp 603−607, Cold Spring Harbor Laboratory Press, Plainview, NY.
39. Burkhoff, A. M., and Tullius, T. D. (1987) *Cell 48*, 935−943.
40. Latham, J. A., and Cech, T. R. (1989) *Science 245*, 276−282.
41. Waugh, D. S., and Pace, N. R. (1993) *FASEB J. 7*, 188−195.
42. Fabrizio, P., and Abelson, J. (1990) *Science 250*, 404−409.
43. Guthrie, C. (1991) *Science 253*, 157−163.
44. Sawa, H., and Abelson, J. (1992) *Proc. Natl. Acad. Sci. U.S.A. 89*, 11269−11273.
45. Sawa, H., and Shimura, Y. (1992) *Genes Dev. 6*, 244−254.
46. Guthrie, C., and Patterson, B. (1988) *Annu. Rev. Genet. 22*, 387−419.
47. Smith, D., and Pace, N. R. (1993) *Biochemistry 32*, 5273−5281.
48. Steitz, T. A., and Steitz, J. A. (1993) *Proc. Natl. Acad. Sci. U.S.A. 90*, 6498−6502.
49. Otzen, D. E., Barciszewski, J., and Clark, B. F. (1994) *Biochemie 76*, 15−21.
50. Zuker, M. (1989) *Science 244* 48−52.
51. Walter, A. E., Turner, D. H., Kim, J., Lyttle, M. H., Mueller, P., Matthews, D. H., and Zuker, M. (1994) *Proc. Natl. Acad. Sci. U.S.A. 91*, 9218−9222.

BI972886Y